Probing Capacitive Coupling and Collective Transport in PbSe Quantum-Dot Arrays Using Scanning Tunneling Spectroscopy

Yi-Ching Ou,[†] Jiun-Ji Wu,[‡] Jiye Fang,[§] and Wen-Bin Jian[‡,*]

Department of Electrophysics and Institute of Physics, National Chiao Tung University, 1001 Ta Hsueh Road, Hsinchu 30010 Taiwan, and Department of Chemistry, State University of New York at Binghamton, Binghamton, New York 13902-6000

Received: January 6, 2009; Revised Manuscript Received: February 7, 2009

Semiconductor quantum dots with diameters of several to tens of nanometers have been largely synthesized through colloidal techniques for nanoscience exploration of quantum confinement, Coulomb staircase, and artificial-atom states in individual quantum dots and self-assembling growth behavior. Although charge transport of three-dimensional quantum dot arrays has been attempted for study on the micron scale, the electrical properties of a nanoscale array, self-assembled from a single quantum dot through a bottom-up procedure, have not been explored yet. We control growth parameters to self-assemble different sizes of PbSe quantum-dot arrays on flat gold surface for scanning tunneling spectroscopy measurements. The current−voltage curves of the arrays are analyzed using a double-barrier tunnel junction model to acquire the shunt capacitance between the array and the gold substrate. The increment of this capacitance is small as the particle number increases extremely from 1 to 40. Thus the array cannot be taken as a simple semiconductor island. We apply collective transport theory to exploration of electron tunneling and capacitive coupling between PbSe quantum dots in the array.

1. Introduction

Few electrons stored on small metal particles or semiconductor quantum dots (QDs) will build a charging energy to block additional electrons' tunneling. This effect is called Coulomb blockage. It changes the conductivity of the current channel due to the small capacitance of the tiny-sized particles which give large blocking Coulomb energy.[1,2] The few-electron charging effects have been applied not only to single-electron transistors but also to the fabrication of single-electron[3,4] and nanocrystal based memories[5,6] for operating at room temperatures. Moreover, another similar phenomenon of electrical bistability exhibits two conductivity states at the same voltage. This nonvolatile electrical bistability has been discovered and demonstrated in the system of nanoclusters embedded in organic or oxide layers.[7,8] Recently, many organic bistable devices, containing different materials of metal particles or semiconductor QDs dispersed in organic layers, have displayed a large hysteresis in current− or capacitance−voltage curves that reveal bistable effects in conductivity and capacitance.[7−10] Although band diagram models have been proposed to explore the device operation mechanism, investigation of the electrical coupling effect among particles from a microscopic viewpoint has not been intended yet.

In recent years, a high temperature organic solution-based wet-chemical strategy has been successfully developed in synthesizing high crystalline QDs in which the surface of particles is passivated by organic ligands.[11] These chemically generated QDs were introduced in a nanogap between metal electrodes for approaches to electrical studies of a single dot[12] and to a single-electron transistor.[13] Meanwhile, the QDs could self-assembled into quasi-one-dimensional chains and two- or three-dimensional arrays. The current−voltage ($I-V$) behavior at various temperatures has been measured for self-assembled chains of conducting carbon nanopartciles[14] and quasi-one-dimensional arrays of gold nanocrystals.[15] In addition, the transport of electrons has been studied in the two-dimensional systems of cobalt-nanocrystal superlattices,[16] Au nanocrystal arrays,[17] CdSe QD arrays,[18] and the topographically complex Au nanoparticle network.[19] These studies reveal a nonlinear $I-V$ curve and a temperature-dependent threshold voltage V_{th} at lower temperatures. In particular, the $I-V$ curves at different temperatures can be collapsed to a single power-law $I(V-V_{th})$ curve by translation on the voltage scale above V_{th}. This behavior is recently exposed in a system of Au nanoparticles self-assembling in organic thin films as well.[20] On the other hand, the scaling behavior has been observed in the early research of lithographically patterned GaAs QDs[21] and Al island arrays.[22] A collective transport model considered by Middleton and Wingreen (MW)[23] can be used to explain the aforementioned experimental results.

In the very early studies, scanning tunneling microscope (STM) has been used to observe the Coulomb blockade characteristics of staircase features on $I-V$ curves of an individual metal droplet or cluster at a very low temperature[24] as well as at room temperatures.[25] Recently, not only the Coulomb effect but also the electronic structures of artificial-atom states in the colloidal and semiconducting QDs were investigated by several research groups[26,27] through measurements of tunneling spectroscopy with the aid of low-temperature STM. In addition to the single-QD electronic states, the interparticle Coulomb interactions[28] and the level structure of InAs QDs in two-dimensional assemblies[29] draw attention for tunneling spectroscopy characterizations. However, the array size effects, which might exhibit during the assembling process from a single QD to a two-dimensional QD array, and the capacitive coupling among the QDs have not been explored to

* To whom correspondence should be addressed. E-mail: wbjian@mail.nctu.edu.tw.
[†] Institute of Physics, National Chiao Tung University.
[‡] Department of Electrophysics, National Chiao Tung University.
[§] Department of Chemistry, State University of New York at Binghamton.

10.1021/jp900131h CCC: $40.75
Published on Web 03/16/2009

date. In this study, we employ STM to probe the size effects in the coupled PbSe QD arrays. The size-dependent tunneling spectra of the QD arrays may give a clue to understand the operation mechanism of memory devices from a microscopic viewpoint.

2. Experimental Section

PbSe QDs were prepared using a high-temperature organic solution approach by adopting a method in previous report.[32] To synthesize PbSe QDs, trioctylphosphine-selenium solution (TOP-Se, 1.0 M for Se) was preprepared as Se-source by dissolving 7.90 g of selenium powder (99.99%) into 100 mL of TOP (90%) in a glovebox and stirring for overnight. In a typical experiment, 1.081 g of lead acetate trihydrate ($PbAc_2 \cdot 3H_2O$, 99.99%, 2.85 mmol), 3.6 mL of oleic acid (90%), and 15 mL of phenyl ether (>99%) were loaded into a flask and heated to 140 °C for 20 min under an argon stream. After the moisture-free solution was cooled to ~40 °C, it was transferred into a glovebox and mixed with 5.0 mL of the TOP-Se stock solution in a syringe. This mixed solution was then rapidly injected into vigorously stirred phenyl ether (15 mL) that was preheated to 200 °C in a three-neck flask equipped with a condenser under argon atmosphere. After the injection, the temperature of the mixture dropped to ~160 °C because of the addition of the room-temperature reagents. Once the solution temperature increased to ~200 °C in ~5 min, the QD growth was terminated by an immediate removal of the heating source. A size-selective precipitation[33,34] was subsequently performed by centrifugation using a pair of solvents consisting of anhydrous hexane (98.5%, BDH) and anhydrous ethanol (200 proof, AAPER). Before the size-selection, the QD average size can also be roughly tuned by varying the QD growth temperature[32] after the injection of the reagents into the hot phenyl ether because raising the solution temperature accelerates the QD growth rate. Solution temperature between 150 and 220 °C was usually chosen to grow the QDs in the desired range of size. The resultant PbSe QDs were identified using various characterizations including X-ray diffraction study, inductively coupled plasma analysis, transmission electron microscope (TEM, JEOL JEM-2010F) imaging, and energy dispersive spectroscopy evaluation. These PbSe QDs generally present in a spherical shape. However, some cubic particles could be detected when the QDs were grown at a temperature of 200 °C or higher. All of the chemicals mentioned above were purchased from Sigma-Aldrich and used as received, except those specified.

To prepare for STM measurements, the QDs were dispersed in toluene again to make a dilute QD solution. Several drops of the solution were put on a conducting and flat substrate. The chosen substrate was atomically flat terraces, with several hundred nanometers in size, on Au(111) surfaces on a ball prepared by melting a 2-mm gold wire in a gas flame. The as-deposited PbSe QDs formed islands with QD numbers from one to several tens and the assembling process can be controlled by the growth conditions of the substrate temperature and the solution concentration. The morphology of QD islands on Au(111) surfaces was inspected by field-emission scanning electron microscope (JEOL, JSM-7000F) and atomic force microscope (Seiko Instruments Inc., SPA-300HV). The sample of as-assembled QD islands was loaded in a STM preparation chamber in an ultrahigh vacuum of 1×10^{-10} torr, and it was heated up to 100−150 °C for more than 10 h. When annealing at 150 °C, long time of thermal treatment helped to detach more organic ligands and to squeeze the distance between QDs. In addition, the PbSe QD islands liquefied and evaporated as the annealing temperature was increased up to 300 °C. The thermal annealing converts the as-assembled QD islands to compact and ordering QD arrays as well. The sample of QD arrays on Au(111) surfaces was transferred to a STM main chamber and the STM analysis were carried out by Omicron LT STM at room temperatures. All STM images were taken in a constant current mode with a sample bias of 2.5 V and a tunneling current (set-point) of 0.15 nA. After the PbSe QD array was specified in a STM topography image, current image tunneling spectroscopy (CITS) will be taken at the same place. The tunneling spectra were taken with voltages ramped from −1.5 to +1.5 V under a scanning condition of the sample bias 1.5 V and the tunneling current 0.15 nA. There were 100 × 100 points in a CITS image and every CITS image point contained an $I-V$ curve having 200 steps. Since the slightly deviated separation distance between the STM tip and the sample could produce a large current fluctuation, the statistically averaged $I-V$ curve from several tens or hundreds of CITS image points was evaluated for an individual PbSe QD array. All the data were analyzed using the software of scanning probe image processor (Image Metrology A/S, SPIP).

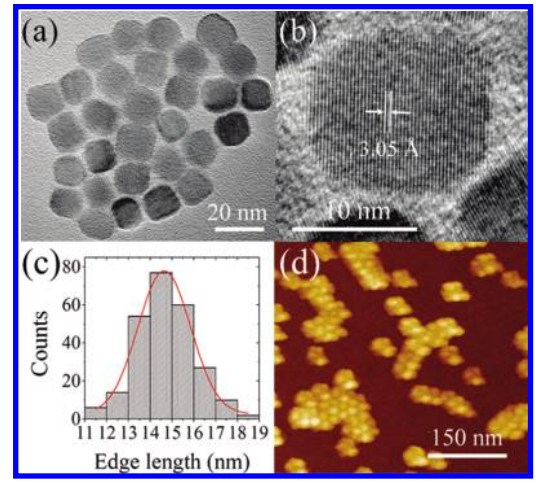

Figure 1. (a) TEM image of PbSe QDs. (b) High-resolution TEM image of an individual PbSe QD. (c) Statistical distribution of QD sizes and a red curve fitted according to a Gaussian function. The average size and standard deviation of the QDs are estimated to be about 14.6 and 2.4 nm, respectively. (d) STM image of PbSe QD arrays dispersing on a gold surface.

3. Results and Discussions

The as-synthesized PbSe QDs are capped with TOP and oleic acid to prevent aggregation. As shown in Figure 1a, the TEM image demonstrates a cluster of PbSe QDs. Since the sample has not been annealed yet, the island does not show apparently the ordering structure among the PbSe QDs. These QDs exhibit either cubic or spherical shapes. A high resolution TEM image of an individual PbSe QD is given in Figure 1b. The image confirms a single crystalline structure with a lattice fringe spacing of 3.05 Å which is in agreement with the lattice constant of the rock salt structure in PbSe bulk. The distribution of QD diameters determined in the TEM images is estimated and presented in Figure 1c. The size distribution can be fitted with Gaussian distribution, yielding a uniform and average diameter of ~14.6 nm and a standard deviation of 17%. Since the average diameter of the PbSe QDs used for this study is larger than 10 nm and the data are taken at room temperatures, it is reasonable to neglect the electronic structure of artificial-atom states in tunneling spectra. In fact, in the same QD system, we have

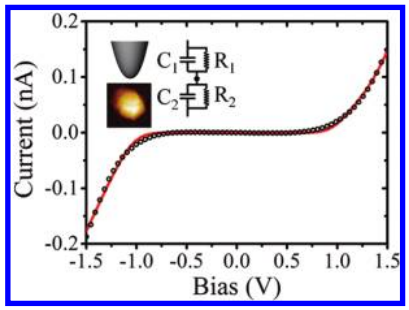

Figure 2. $I-V$ curve of the single PbSe QD on the gold surface. The open circles denote experimental data, and the red line gives the best fit to the orthodox theory. The insert gives a scheme of a tip and an STM image (44×44 nm^2) showing the single PbSe QD on which the $I-V$ curve is taken. A circuit diagram is shown in the insert as well.

observed the feature of artificial-atom states in $I-V$ curves only at ~5 K. To investigate the electronic structure of these QD arrays using an STM, PbSe QDs are deposited on a conducting substrate. The QDs will form clusters as well as islands on the substrate with different sizes and shapes owing to different packing conditions. Figure 1d shows a typical STM image of PbSe QD arrays on a flat Au(111) surface. Since the thermal annealing in an ultrahigh vacuum has been applied to the gold substrate, the QD islands exhibit a much more ordered arrangement compared to that displayed in Figure 1a.

We examined $I-V$ behavior of a single QD and analyzed the data based on the orthodox theory[30] of correlated electron tunneling before investigating the electronic structure of the PbSe QD arrays. The STM image of a single QD and the double-barrier tunnel junction model for the orthodox theory are given in the inset of Figure 2. A STM tip is schematically drawn above the STM image of the single QD to illustrate the corresponding tip-to-dot and the dot-to-substrate resistances (R_1 and R_2) and capacitances (C_1 and C_2) in the circuit diagram. Figure 2 displays data points of an $I-V$ curve for the single QD shown in the inset. The data are averaged from 221 $I-V$ curves as well as CITS image points, and they exhibit a large Coulomb blockade with a V_{th} of about 1 V. In this study, gate voltage induced polarization charge Q_0 can be small enough so that a larger V_{th} was able to be observed. In addition, both experimental data and fitting curve show rounded $I-V$ at V_{th} owing to thermal fluctuations at room temperatures. The experimental data can be fitted with the orthodox theory at 300 K to give a polarization charge Q_0 of 0.07 e, R_1 and R_2 of 2.18 and 1.14 GΩ, and C_1 and C_2 of 0.065 and 0.071 aF, respectively. The parameters justify the V_{th} of 0.96 V according to the relation $V_{th} = (0.5e + Q_0)/\max\{C_1,C_2\}$, where e is the electron charge.[31] Both R_1 and R_2, the shunt resistances, are larger than the quantum resistance h/e^2 (where h is Plank's constant), to ensure the electron tunneling rather than the forming of conduction channels among the STM tip, PbSe QD, and substrate. The charging energy estimated from the shunt capacitances C_1 and C_2 is 588 meV, which is considerably large in contrast with a thermal energy of ~25 meV at room temperatures, so the Coulomb blockade effect is robust and detectable. In comparison with a previous report,[25] the capacitances C_1 and C_2 are in the same order of magnitude while the resistance R_2 is 1000 times higher, implying an existence of organic ligands, such as TOP and oleic acid, between the QD and the substrate even after ultrahigh vacuum annealing.

The analysis of the tunneling spectrum of a single PbSe QD shows that our tip−QD−substrate system can be modeled by the double-barrier tunnel junction model and the orthodox

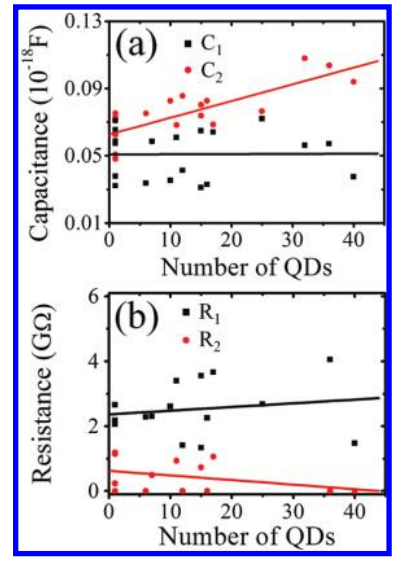

Figure 3. Shunt capacitances C_1 and C_2 (a) and resistances R_1 and R_2 (b), estimated from fittings with the orthodox theory, revealing a dependence on the number of QDs. The approaching lines only give a guide to the eye.

theory. Thus, we turn to examine the tunneling spectra of QD arrays. To analyze the tunneling spectra using the orthodox theory, we start with the assumption of taking the QD array as a simple island. Several hundred of CITS image points ($I-V$ curves) are averaged to get one characteristic $I-V$ curve. The $I-V$ curve of a specified QD array is fitted to obtain the double-junction parameters, C_1, C_2, R_1, and R_2. The parameters of shunt capacitances and resistances as a function of sizes (QD numbers) are given in Figure 3, panels a and b, respectively. As the QD number increases from 1 to 40, the tip-to-array capacitance C_1 remains constant (~0.05 aF) while the array-to-substrate capacitance C_2 steadily rises from ~0.06 to ~0.10 aF. The constant C_1 suggests that the STM tip could be modeled as a sphere with a lateral dimension which is almost the same as the QD diameter. The increment of the QD number does not change the effective area of the tip-to-array capacitance so the C_1 keeps the same value. On the other hand, the effective area of the array-to-substrate capacitance expands about 40 times but the C_2 only duplicates its value. The retarded ascent of the C_2 implies that the QD array cannot be taken as a simple island. Unlike previously observed phenomena of delocalized electrons and holes among the QDs,[28,29] the electron and hole in the PbSe QD can only tunnel to, or introduce polarization charges in, neighboring QDs instead of forming direct conducting channels. The tunneling and capacitive coupling among PbSe QDs could lead to collective transport, which will be discussed later, in the QD arrays. Like the behavior of the C_1, the tip-to-array resistance R_1 seems to be independent of the number of QDs in the array because the scanning parameters, such as the tunneling current and sample bias, remain the same to keep a separation distance between the STM tip and the QD array. On the other hand, the averaged array-to-substrate resistance R_2 decreases moderately from ~0.61 to ~0.056 GΩ. The apparent diminution of the R_2 could stem from parallel-connected tunneling resistances among the PbSe QDs and between the QDs and the substrate.

To corroborate the conclusion that the QD array cannot be regarded as a simple island, we go back to examine the separation distance between the QDs from the STM measurements. By using the fast Fourier transform technique, we can find ordering dots or a ring structure with a radius on the

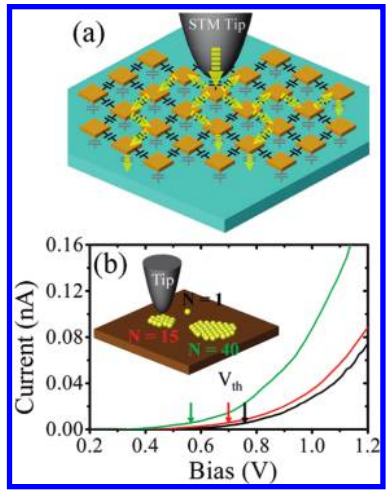

Figure 4. (a) Schematic diagram of the model of a STM tip on a PbSe QD array. The brown lumps represent QDs and the dot-to-dot and dot-to-substrate capacitances are indicated by black and gray lines, respectively. The yellow dashed lines and arrows hint the electrons' tunneling. (b) $I-V$ curves of arrays with QD numbers of 1, 15, and 40. The threshold voltages V_{th}'s are indicated on the $I-V$ curves. The scheme of our experiment is drawn in the inset.

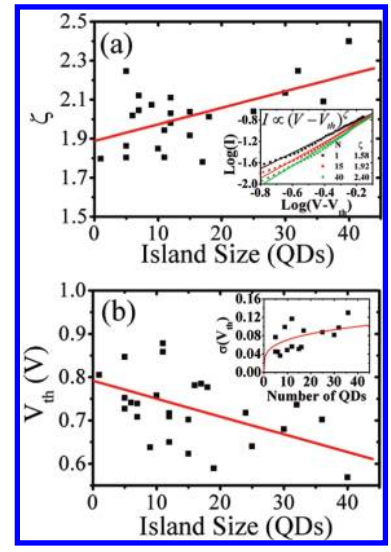

Figure 5. (a) Scaling exponent ζ as a function of QD number and a red line indicating a boosting tendency. The inset displays the power law behavior $I(V-V_{th})$ of the $I-V$ curve in a logarithmic scale with scaling exponents of 1.58, 1.92, and 2.40 for arrays with QD numbers of 1, 15, and 40, respectively. (b) The V_{th} as a function of QD numbers and a red line indicating a declining tendency. The inset gives the standard deviation $\sigma(V_{th})$ of the fluctuation in the V_{th}'s for individual QDs in the array. A red curve depicts a tendency of a power law function of the QD number with an exponent of 1/4.

transformed image and estimate the average center-to-center distance of 16.3 ± 0.4 nm. The separation distance between two QDs can be evaluated to be about 1.7 nm which guarantees that the two QDs are still in the tunneling regime. In addition, we assume that the QDs have a cubic structure with a square face area A of ~214 nm^2 and the QDs are arranged to admit a face-to-face separation distance d of ~1.7 nm. By using the model of parallel plate capacitor, we can estimate the dot-to-dot coupling capacitance $C_{ij} = (\varepsilon_r\varepsilon_0 A)/d$ to be about 2.26 aF, where ε_0 is the dielectric constant in vacuum and ε_r is 2.1 for organic ligands (TOP).[16,35,36] In Figure 4a, we illustrate electron transport in this particular system consisting of a STM tip, a PbSe QD array, and a substrate. The electrons tunnel from the STM tip to one of the PbSe QD in the array while the electrons in the tip-positioned PbSe QD couples to neighboring QDs through electron tunneling and interdot capacitor C_{ij} induced polarization. Since every QD may have a different polarization charge Q_0 to render a disorder in the QD array, we may adopt MW model[23] to analyze collective transport in this system. In particular, unlike the parallel array discussed in the model that has one dimension in parallel with electron transport direction, our system, comprising two dimensions in perpendicular to electron transport direction, can be regarded as a perpendicular array. The interdot capacitance C_{ij} provides a charging energy of ~35 meV which supports the feasible observance of collective transport at room temperatures. In addition, the interdot capacitance (2.26 aF) is much larger than either the tip-to-array or the array-to-substrate capacitances (C_1 and C_2) to ensure a long screening length and a strong capacitive coupling ($C_{ij} \gg C_1$ or C_2) in the QD array. Figure 4b presents $I-V$ curves of PbSe QD arrays with QD numbers of 1, 15, and 40, and the inset illustrates the corresponding tip−array−substrate systems. To evaluate the V_{th}'s for QD arrays, $I-V$ curves of six different single QDs are acquired and fitted with the orthodox theory (see previous discussions for Figure 2) to evaluate the V_{th}'s and threshold currents. The averaged threshold current of ~5.5 pA of the single QD is used to evaluate the V_{th}'s of all of the other QD arrays. The V_{th}'s indicated in Figure 4b are 0.77, 0.70, and 0.57 V for arrays with QD numbers of 1, 15, and 40, respectively. The feature that V_{th} does not fall dramatically with an increase of QD numbers from 1 to 40 implies again that the QD array cannot be simply treated as a single island.

The MW model predicts that the $I-V$ characteristics obey a scaling law of $I \propto (V\text{-}V_{th})^{\zeta}$ at voltages above V_{th}, where ζ is the scaling exponent. After the V_{th}'s of PbSe QD arrays have been evaluated, the $I-V$ curves can be translated on the voltage scale and fitted with the scaling law to get the scaling exponent ζ. The translated $I(V\text{-}V_{th})$'s of arrays with three different QD numbers are exposed in the inset of Figure 5a. Through a linear least-squares fitting in the logarithmic scale, the scaling exponents of 1.58, 1.92, and 2.4 are estimated for arrays with QD numbers of 1, 15, and 40, respectively. The value of scaling exponent estimated from our STM configuration is in the range of 1.5−2.5 which covers the value for the two-dimensional parallel arrays in theory[23] and for quasi-one- and two-dimensional cases in experiments.[14−19] Moreover, Figure 5a presents, for the first time, the size (QD number) dependence of the scaling exponent ζ. It gradually increases with an enlarging size of the PbSe QD array. For the single QD array, one channel opens between the tip and the substrate through the PbSe QD. When the array size increases, more and more possible channels, from the tip-positioned QD to the neighboring QDs, will open to increase the current and raise the scaling exponent ζ. Until now, there is no theoretical prediction of the ζ for a three-dimensional case and for our two-dimensional perpendicular arrays in which the electron transport direction is perpendicular to the QD array. On the other hand, the size dependence of threshold voltages V_{th}'s is given in Figure 5b demonstrating a gradual recession from 0.8 to 0.6 V as the number of QDs increases from 1 to 40. The tendency of the decreasing V_{th} seems to be in line with the increment of the array-to-substrate capacitance C_2 introduced in Figure 3a. Furthermore, the V_{th} of an individual QD in an array is acquired for calculation of the standard deviation $\sigma(V_{th})$ of the fluctuation in the V_{th}. The size dependent fluctuation $\sigma(V_{th})$ is plotted in the inset of Figure 5b and the fitting curve displays the tendency of a power law function with an exponent of 1/4. In comparison

with a theoretical prediction of an exponent 1/2 for a parallel array[23] having a length of one QD between two leads, the fluctuation $\sigma(V_{th})$ is depressed in the particular system of perpendicular arrays.

4. Conclusion

In summary, the PbSe QDs self-assemble to form arrays with different sizes (QD numbers) on flat Au(111) surfaces and the scanning tunneling spectra of individual QD arrays are measured using STM. The average $I-V$ curve of a single PbSe QD can be fitted with the orthodox theory to get the shunt resistances and capacitances of the double-barrier tunnel junction model. In addition, the array-to-substrate shunt capacitance of the QD array is estimated to discern a small increment with a large increase of QD numbers from 1 to 40. The retarded increase of the array-to-substrate capacitance implies that the QD array can be neither treated as a simple island nor taken as independent QD. Therefore, the MW model of collective transport might be used to examine the scanning tunneling spectra. After fitting with the MW model, we identify that the $I(V-V_{th})$ curves of the QD arrays follow a power law with a scaling exponent ζ after translation on the voltage scale with the threshold voltage V_{th}. The scaling exponent ζ increases but the threshold voltage V_{th} decreases with the increasing size and the QD number of the arrays. The fluctuation in the threshold voltage V_{th} has been unprecedentedly estimated to show a power law function of the QD number with an exponent of 1/4 for the particular system of perpendicular PbSe QD arrays.

Acknowledgment. The authors thank Prof. Juhn-Jong Lin for using his facilities. This work was supported by the Taiwan National Science Council under Grant No. NSC 95-2112-M-009-045-MY3 and by the MOE ATU Program. J.F. thanks U.S. NSF support (DMR-0731382).

References and Notes

(1) Likharev, K. K. *Proc. IEEE* **1999**, *87*, 606.
(2) Laibowitz, R. B.; Stiles, P. J. *Appl. Phys. Lett.* **1971**, *18*, 267.
(3) Yano, K.; Ishii, T.; Hashimoto, T.; Kobayashi, T.; Murai, F.; Seki, K. *IEEE Trans. Electron Devices* **1994**, *41*, 1628.
(4) Guo, L.; Leobandung, E.; Chou, S. Y. *Science* **1997**, *275*, 649.
(5) Tiwari, S.; Rana, F.; Hanafi, H.; Hartstein, A.; Crabbe, E. F.; Chan, K. *Appl. Phys. Lett.* **1996**, *68*, 1377.
(6) Fischbein, M. D.; Drndic, M. *Appl. Phys. Lett.* **2005**, *86*, 193106.
(7) Ma, L.; Pyo, S.; Ouyang, J.; Xu, Q.; Yang, Y. *Appl. Phys. Lett.* **2003**, *82*, 1419.
(8) Ouyang, J.; Chu, C.-W.; Sieves, D.; Yang, Y. *Appl. Phys. Lett.* **2005**, *86*, 123507.
(9) Jung, J. H.; Jin, J. Y.; Lee, I.; Kim, T. W.; Roh, H. G.; Kim, Y.-H. *Appl. Phys. Lett.* **2006**, *88*, 112107.
(10) Li, F.; Son, D.-I.; Ham, J.-H.; Kim, B.-J.; Jung, J. H.; Kim, T. W. *Appl. Phys. Lett.* **2007**, *91*, 162109.
(11) Alivisatos, A. P. *Science* **1996**, *271*, 933.
(12) Klein, D. L.; McEuen, P. L.; Bowen Katari, J. E.; Roth, R.; Alivisatos, A. P. *Appl. Phys. Lett.* **1996**, *68*, 2574.
(13) Klein, D. L.; Roth, R.; Lim, A. K. L.; Alivisatos, A. P.; McEuen, P. L. *Nature* **1997**, *389*, 699.
(14) Bezryadin, A.; Westervelt, R. M.; Tinkham, M. *Appl. Phys. Lett.* **1999**, *74*, 2699.
(15) Elteto, K.; Lin, X. M.; Jaeger, H. M. *Phys. Rev. B* **2005**, *71*, 205412.
(16) Black, C. T.; Murray, C. B.; Sandstrom, R. L.; Sun, S. *Science* **2000**, *290*, 1131.
(17) Parthasarathy, R.; Lin, X. M.; Elteto, K.; Rosenbaum, T. F.; Jaeger, H. M. *Phys. Rev. Lett.* **2004**, *92*, 076801.
(18) Romero, H. R.; Drndic, M. *Phys. Rev. Lett.* **2005**, *95*, 156801.
(19) Blunt, M. O.; Suvakov, M.; Pulizzi, F.; Martin, C. P.; Pauliac-Vaujour, E.; Stannard, A.; Rushforth, A. W.; Tadic, B.; Moriarty, P. *Nano Lett.* **2007**, *7*, 855.
(20) Li, C. P.; Wu, C. H.; Wei, K. H.; Sheu, J. T.; Huang, J. Y.; Jeng, U. S.; Liang, K. S. *Adv. Funct. Mater.* **2007**, *17*, 2283.
(21) Duruoz, C. I.; Clarke, R. M.; Marcus, C. M.; Harris, J. S. *Phys. Rev. Lett.* **1995**, *74*, 3237.
(22) Rimberg, A. J.; Ho, T. R.; Clarke, J. *Phys. Rev. Lett.* **1995**, *74*, 4714.
(23) Middleton, A. A.; Wingreen, N. S. *Phys. Rev. Lett.* **1993**, *71*, 3198.
(24) Wilkins, R.; Ben-Jacob, E.; Jaklevic, R. C. *Phys. Rev. Lett.* **1989**, *63*, 801.
(25) Andres, R. P.; Bein, T.; Dorogi, M.; Feng, S.; Henderson, J. I.; Kubiak, C. P.; Mahoney, W.; Osifchin, R. G.; Reifenberger, R. *Science* **1996**, *272*, 1323.
(26) Banin, U.; Cao, Y.; Katz, D.; Millo, O. *Nature* **1999**, *400*, 542.
(27) Liljeroth, P.; van Emmichoven, P. A. Z.; Hickey, S. G.; Weller, H.; Grandidier, B.; Allan, G.; Vanmaekelbergh, D. *Phys. Rev. Lett.* **2005**, *95*, 086801.
(28) Liljeroth, P.; Overgaag, K.; Urbieta, A.; Grandidier, B.; Hickey, S. G.; Vanmaekelbergh, D. *Phys. Rev. Lett.* **2006**, *97*, 096803.
(29) Steiner, D.; Aharoni, A.; Banin, U.; Millo, O. *Nano Lett.* **2006**, *6*, 2201.
(30) Amman, M.; Wilkins, R.; Ben-Jacob, E.; Maker, P. D.; Jaklevic, R. C. *Phys. Rev. B* **1991**, *43*, 1146.
(31) Wang, L.; Taylor, M. E.; Welland, M. E. *Surf. Sci.* **1995**, *322*, 325.
(32) Murray, C. B.; Sun, S.; Gaschler, W.; Doyle, H.; Betley, T. A.; Kagan, C. R. *IBM J. Res. Dev.* **2001**, *45*, 47.
(33) Sun, S.; Murray, C. B. *J. Appl. Phys.* **1999**, *85*, 4325.
(34) Murray, C. B.; Kagan, C. R.; Bawendi, M. G. Annu. *Rev. Mater. Sci.* **2000**, *30*, 545.
(35) Leatherdale, C. A.; Bawendi, M. G. *Phys. Rev. B* **2001**, *63*, 165315.
(36) Blanton, S. A.; Leheny, R. L.; Hines, M. A.; Guyot-Sionnest, P. *Phys. Rev. Lett.* **1997**, *79*, 865.

JP900131H